

1 **Estimating changes in temperature distributions in a large ensemble of**
2 **climate simulations using quantile regression**

3 Matz A. Haugen*, Michael L. Stein and Elisabeth J. Moyer

4 *University of Chicago, Chicago, USA*

5 Ryan L. Sriver

6 *University of Illinois at Urbana-Champaign, Urbana, USA*

7 *Corresponding author address: Matz A. Haugen, 5734 S. Ellis Ave, 60637, Chicago, USA.

8 E-mail: mahaugen@uchicago.edu

ABSTRACT

9 Understanding future changes in extreme temperature events in a transient
10 climate is inherently challenging. A single model simulation may be insuffi-
11 cient to characterize the statistical properties of the underlying physical pro-
12 cesses governing the climate. Ensembles of repeated simulations with differ-
13 ent initial conditions greatly expand the amount of data available, which in
14 turn enables new approaches for characterizing changes in extremes. Here
15 we present one such new approach, focusing on quantiles and differences in
16 quantiles as ways of describing how temperature distributions change over
17 time. Specifically, we use quantile regression to estimate temperature distri-
18 butions as continuous functions of day of year and year rather than breaking
19 the dataset into seasonal blocks. To demonstrate our method’s utility, we an-
20 alyze an ensemble of 50 simulations of the Community Earth System Model
21 (CESM) under a scenario of increasing radiative forcing to 2100, focusing
22 on North America. As previous studies have found, we see that daily tem-
23 perature bulk variability generally decreases in wintertime in the continental
24 mid- and high-latitudes ($> 40^\circ$). A more subtle result that our approach un-
25 covers is that differences in two low quantiles of wintertime temperatures do
26 not shrink as much as the rest of the temperature distribution producing a
27 more negative skew in the overall distribution. Although the examples above
28 concern temperature only, the technique is sufficiently general that it can be
29 used to generate precise estimates of distributional changes in a broad range
30 of climate variables by exploiting the power of ensembles.

31 **1. Introduction**

32 Time series of climate variables have generally been assumed to be separable into two compo-
33 nents: randomness inherent in the underlying physical processes, which we call natural variability,
34 and climatic trends, which we take to include seasonality and forced secular trends that follow from
35 increasing concentrations of greenhouse gases. Recently, the degree to which natural variability
36 may itself be changing has received significant scientific interest (e.g. Trenberth 2011; Donat and
37 Alexander 2012; Deser et al. 2012a; Thompson et al. 2015; Kay et al. 2015). Potential changes in
38 climate extremes, because of their heightened societal impacts, are of special concern (e.g. Davi-
39 son and Smith 1990; Stott et al. 2004; Chavez-Demoulin and Davison 2005; Eastoe and Tawn
40 2009; Otto et al. 2012; Swain et al. 2014; Singh et al. 2014; Trenberth et al. 2015; Diffenbaugh
41 et al. 2015; Huang et al. 2015a; Jalbert et al. 2017). However, fully characterizing this evolving
42 natural variability of rare events is intrinsically challenging due to the limited amount of available
43 observations or simulation data. The long equilibration time of the climate system means that on
44 the timescales of interest to human society, the climate state will be evolving, so that its statistical
45 properties are not stationary. Studies of future climate extremes often employ statistical extreme
46 value theory to make inferences about rare events with modest amounts of data (Swain et al. 2014).

47 In this work, we study the entire distribution of temperatures in a transient climate, including
48 rare events, by employing quantile regression on an ensemble of simulations of an identical forc-
49 ing scenario from a single climate model. Sufficient sampling of the initial conditions' uncertainty
50 will reflect the natural variability of the climate system, since each simulation is statistically in-
51 dependent in terms of its natural variability. The increased data provided by multiple simulations
52 enables more confident statements about changes in the statistical behavior of the system than can
53 be made with a single simulation. The use of initial conditions for characterizing internal vari-

54 ability is growing rapidly (e.g. Deser et al. 2012b,a, 2014; Fischer and Knutti 2014; Kay et al.
55 2015; Srivastava et al. 2015; Rodgers et al. 2015; Hagos et al. 2016). Deser et al. (2012b), Deser
56 et al. (2012a) and Fischer and Knutti (2014) in particular discuss how ensembles help distinguish
57 internal climate variability from anthropogenic effects on temperature changes and allow more
58 comprehensive estimates of the model's temperature response to radiative forcing.

59 Large single model ensembles offer at least three advantages over a single simulation of a climate
60 model. The most obvious advantage is that the increased data volume allows closer examination
61 of the entire distribution of a climate variable. Studies of climate variability to date are generally
62 divided between those that address the center of the distribution (e.g. Semenov and Bengtsson
63 2002; Räisänen 2002; Kitoh and Mukano 2009; Screen 2014; Schneider et al. 2015), and those
64 that address its tails (e.g. Katz and Brown 1992; Meehl et al. 2009; Northrop and Jonathan 2011;
65 Davison et al. 2012; Huser and Davison 2014; Trenberth et al. 2015; Huang et al. 2015b; Jal-
66 bert et al. 2017), generally via extreme value theory. A more limited body of studies address
67 overall distributional changes in climate variables, but these generally focus on observations or
68 observation-based data products, which are necessarily limited in terms of data amount and there-
69 fore require spatial or temporal aggregation (Donat and Alexander 2012; Stainforth et al. 2013;
70 Chapman et al. 2013; Huybers et al. 2014; McKinnon et al. 2016; Rhines et al. 2017). Aggregating
71 data spatio-temporally requires stationarity assumptions of the signal or explicitly modeling the
72 spatio-temporal structure. When studying model projections using ensembles, the large amounts
73 of data at each location allows us to estimate changes in the distribution of climate variables (e.g.
74 temperature) without spatial aggregation.

75 A second advantage provided by large single model ensembles is that trends in both means
76 and variability need not be modeled as linear in time (Franzke 2015; Gao and Franzke 2017).
77 Forcings are not linear over centennial timescales, and a linear approximation can be misleading

78 (see for example Poppick et al. 2017). The increased data provided by ensembles allows more
79 flexible statistical models to represent complex climate responses. As we will show, distributions
80 of daily temperature evolve nonlinearly, and follow different trajectories for different quantiles
81 (i.e. different parts of the distribution). Analysis methods should therefore be able to take into
82 account nonlinearities both in time and across quantiles.

83 Finally, a third advantage of ensembles is that they allow a more natural treatment of seasonal
84 variation in climate variables. In situations of limited data, it is standard practice to treat seasons
85 separately, assuming that each season has a temporally constant average and stationary statistical
86 properties discontinuous from neighboring seasons. With ensembles of simulations, we can allow
87 for a smooth change in the underlying trend from day to day, using a parsimonious set of param-
88 eters. By modeling the entire year on a continuum, we can explore how each season transitions
89 to the next and how seasonal patterns change over time, features that may be highly dependent on
90 both geographic location and quantile.

91 We describe here a methodology for exploiting ensembles to study changing climate variabil-
92 ity that captures these advantages: we model the complete distribution of daily temperatures as
93 a continuous function of both seasonality and secular climate change over time. We also show
94 how such an ensemble-based approach is well-positioned for the purposes of uncertainty quan-
95 tification. Because each simulation is treated as an independent sample drawn from the ensemble
96 of simulations, we can obtain uncertainty quantifications for all estimates by resampling com-
97 plete simulations from the ensemble without having to model temporal dependence within each
98 simulation.

99 In the sections that follow, we describe estimated changes in both bulk and tail variability as
100 differences in two quantiles; a large quantile difference implies more variability in a given part
101 of the distribution. When, for example, both of those quantiles lie in the low tail, the quantile

102 difference is a measure of the spread or thickness of the lower tail. Figure 1 gives a pictorial
103 explanation of how quantile differences reflect bulk and tail variability. When applied to model
104 runs of a realistic future climate scenario, results reproduce some well-understood changes (e.g.
105 strong reduction in wintertime variability at continental mid-latitudes) and produce some new
106 insights (e.g. strong changes in skewness driven by low tail behavior).

107 While the focus on quantiles and quantile differences makes the use of quantile regression nat-
108 ural, it is possible to estimate quantiles using empirical distributions of temperatures within, say,
109 seasonal blocks for each decade, and use these results to study how quantile differences change
110 over time. Even if ignoring changes in quantiles within a season is viewed as satisfactory, we
111 prefer the quantile regression approach with carefully chosen covariates to capture seasonal and
112 long-term trends outlined in Section 3. For example, in Section 4, we show how the first day of the
113 year at which a range of estimated quantiles cross certain temperature thresholds evolve over time
114 at a site, which is not a question that can be answered when fitting a single temperature distribution
115 for each season.

116 **2. Data**

117 We apply our algorithm to an ensemble of 50 historical/future simulations of the Community
118 Earth System Model (CESM) (Sriver et al. 2015). The atmospheric component is the low-
119 resolution Community Atmosphere Model version 4, with T31 spectral resolution ($\sim 3.75^\circ \times$
120 3.75°) and 26 vertical levels. The model ocean component is the low-resolution version of the
121 Parallel Ocean Program version 2 (Smith et al. 2010) with a nominal horizontal grid resolution of
122 3° , augmented to approximately 1° at the equator. The ocean model contains 60 vertical levels,
123 down to a maximum depth of 5,500 m.

124 The ensemble is appropriate for the purpose of studying coupled internal climate variability
125 because it is based on a $\sim 10,000$ year pre-industrial control simulation. After a ~ 4000 year spin-
126 up using constant preindustrial conditions, 50 historical hindcasts (1850-2005) are initialized from
127 snapshots of the coupled model state taken every 100 years, so that the last hindcast is initialized
128 after approximately 9000 years of the control simulation. Each hindcast is then extended to 2100
129 using the Representative Concentration Pathway (RCP) 8.5 scenario. The 100-year gap between
130 each new initialization ensures nearly independent ensemble members that fully capture internal
131 variability within the coupled system. RCP8.5 corresponds to anthropogenic radiative forcing of
132 roughly 8.5 W m^{-2} by 2100 (Moss et al. 2010). More information about the model and ensemble
133 design can be found in Srivver et al. (2015).

134 CESM does show some known biases that affect primarily temperature means (and possibly
135 trends in means), but also to some extent the higher-order moments of the temperature distribution,
136 e.g. variance and skewness. Known model biases include reduced ocean heat transport, low north
137 Atlantic sea surface temperature, and excessive northern hemisphere sea ice (Shields et al. 2012).
138 The model generally underestimates both temperature and precipitation extremes compared with
139 observations, i.e. the mean of the extreme value distributions is biased, but the scale and shape are
140 consistent with observations for the continental United States (Srivver et al. 2015).

141 In assessing the practical relevance of our results on the shapes of temperature distributions, it
142 is perhaps helpful to compare CESM temperatures with those from the ERA-Interim (European
143 Reanalysis) data product (Dee et al. 2011). Figure 2 shows the model/reanalysis comparison for
144 winter; for summer see Supplementary Online Material Figure S1. The model underestimates
145 variability in some places, and produces excessively cold winter temperatures in the Arctic. The
146 resulting temperature gradients contribute to excess variability and negative skew in the northern
147 mid-latitudes. Skewness is proportional to the cube of temperature after subtracting off the average

seasonal temperature; see Appendix A1. We see that, despite some discrepancies, Figure 2 shows the model runs do a good job overall of capturing where wintertime skewness is positive and negative. Throughout this work, we will show in-depth analysis from three locations with distinct temperature distributions to highlight our proposed method (**a**, **b**, and **c** shown in Figure 2). See Supplementary Online Material Figure S2 for comparison of model and reanalysis temperature distributions in both summer and winter for these locations.

3. Methods

In the methodology presented here, we model temperature at each location as a function of both seasonality and long-term change of the annual temperature distribution. We use two independent variables, with seasonality represented by a variable d , the day of the year (spanning values 1 to 365), and change in annual temperature represented by a variable t , years elapsed since 1850 (spanning 0 to 250 for these scenarios). We thus assume that each temperature quantile can be described by two sets of basis functions that represent the two variables' independent relationships with temperature (called here $\{f_i(d)\}$ and $\{g_j(t)\}$), and interaction terms $h_i(d)s_j(t)$, where f_i, g_j, h_i , and s_j are all smooth functions of the appropriate variable. The interaction terms are required to capture effects in which long-term temperature evolution differs between seasons, e.g. the robust projection that winter temperatures warm more than summer temperatures. To impose our smoothness condition, we assume that f_i, g_j, h_i , and s_j are cubic splines, which are piecewise cubic polynomials with a continuous second derivative (For a review of cubic polynomial basis functions, see Hastie et al. 2009, Chapter 5.) Because the seasonality variable d is periodic, its basis functions are also assumed periodic. For more details, see Appendix A2a.

We choose the number of basis functions by evaluating a metric representing model adequacy. Our model sufficiency criterion is aimed at capturing the long term underlying signal. We do not

require estimated quantile functions to capture transient events during the historical period like volcanic eruptions. Details on how we select the number of basis functions is given in Appendix A2b. In our climate simulation output, the intra-seasonal effect requires more detailed modeling than the inter-seasonal effect. In the results shown here, we fit the model with 15 terms (that is, basis functions) for the main seasonal effect $\{f_i\}$, but the interaction terms require less seasonal complexity, so we use only 3 terms for $\{h_i\}$. We use 4 terms for both the temporal change $\{g_j\}$ and the interaction terms $\{s_j\}$. That is, modeling long-term change generally requires fewer terms than modeling seasonality. In summary, we use 32 basis functions in total including an intercept term. We then fit each q quantile of temperature

$$T_q(d, t) = \alpha + \sum_i a_i f_i(d) + \sum_j b_j g_j(t) + \sum_{i,j} c_{i,j} h_i(d) s_j(t), \quad (1)$$

where all of the coefficients depend on q but we suppress the dependence for convenience. This fit determines coefficients $\alpha, a_i, b_j, c_{i,j}$ for each quantile at each location.

To simplify notation, we construct a matrix X where each column contains a basis function and each row refers to a unique value of d, t and ensemble member. Using this matrix we construct our temperature model in vectorized form,

$$T_q = X\beta_q, \quad (2)$$

where β_q contains the 32 basis coefficients $\alpha, a_i, b_j, c_{i,j}$. The predictor matrix X has 32 columns, each corresponding to one basis function, and $365 \times 250 \times 50$ rows. To get a confidence interval for each entry of T_q , we re-estimate the coefficients, β_q , using a resampled data set. Because we have 50 simulations we resample the data by drawing whole simulations from our ensemble of 50 simulations. By resampling complete realizations, the dependency structure within realizations is maintained in the resampled data. Repeating this resampling and re-estimation procedure 100

191 times yields pointwise confidence bands around each estimated T_q . Appendix A2c provides further
192 details about uncertainty quantification.

193 As an example of a typical model fit, we show in Figure 3 the seasonal cycle in CESM daily
194 temperatures for three locations, along with estimates of low, median and high quantiles. We show
195 here data from 1850 to demonstrate the seasonal fit rather than that of the long-term trend. All
196 locations show strong seasonal differences in variance that are well-represented by our smooth
197 estimates. Relevant features that are captured include an asymmetrical seasonal cycle in all loca-
198 tions; a clear left skewness in wintertime in all three locations (although most pronounced in the
199 higher-latitude **a** and **b**); and a distinct springtime shoulder in the higher-latitude locations. These
200 characteristics show the benefit of explicitly modeling seasonal variations as smoothly varying
201 functions as opposed to a set of four constant functions changing with the seasons. Nuances like
202 the decrease in winter temperature spread (variability) from early to late winter would not be cap-
203 tured by a piecewise constant model.

204 **4. Results and Discussion**

205 To facilitate comparison with previous studies, we first perform a preliminary analysis where
206 we replicate more standard methods. That is, we examine changes in the aggregate distribution
207 of temperatures over multi-week and multi-month intervals, before we show results from our new
208 approach that calculates responses for individual days. Even the standard analysis readily shows
209 that temperature distributions in the CESM ensemble change over the RCP 8.5 scenario (Figures
210 4, 5, and 6, which compare the initial and final time windows 1850-1864 and 2086-2100). Means
211 uniformly shift to warmer temperatures, but the shapes of the distributions also change in terms of
212 variance and skewness. Figure 4 shows initial and final distributions in our example locations for
213 aggregated 15-day periods in winter and summer. In at least two of the three depicted locations,

214 it is clear that the distributions are becoming narrower, although quantifying exactly how the tails
215 are changing requires a quantification of the tail size and shape.

216 Regarding the spatial characteristics of temperature distributions, we see the expected strong
217 decrease in variance in winter over land, especially in the northern mid-latitudes (Figures 5 and 6).
218 By contrast, summer variance changes are much smaller and differ in sign in different locations.
219 Temperature skewness, i.e. the asymmetry of the distribution, shows strong changes in winter
220 over land in a dipole pattern. Winter temperature distributions are in all time periods negatively
221 skewed throughout most of the domain, but in the north (including locations **a** and **b**), they become
222 more negatively skewed in the future, while in the south (including location **c**), they become more
223 symmetric. Summer skewness changes are again smaller and with less spatial coherence, other
224 than the strong transitions in the Southern Great Plains and in Mexico/Central America, where
225 skewness in temperature distributions actually changes sign.

226 Our methodology for quantile estimation provides additional information that helps to quantify
227 how temperature distributions are changing and to estimate the uncertainty associated with each
228 change. We can evaluate not only bulk variability – the interquartile range (IQR), the difference
229 between the 0.25 and 0.75 quantiles – but differences between any two quantiles. Denote by
230 Δq_l the difference between estimated 0.05 and 0.025 quantiles, and Δq_h , the difference between
231 estimated 0.975 and 0.95 quantiles. These quantities measure tail variability in the same way
232 that interquartile range measures the variability of the bulk distribution. If the skewness of a
233 distribution changes over time, then future distributions are not simply scaled versions of present
234 distributions. That is, their tail variabilities must change by a different factor than the IQR. In
235 the case of the northern mid-latitudes winter temperatures shown in Figure 5, where distributions
236 become more negatively skewed as bulk variability decreases in the future, the effect could result

from either a low tail contracting less than the bulk (or actually increasing), and/or a high tail contracting more than the bulk. Our methodology allows readily differentiating these cases.

To assess whether the high tail and/or the low tail is driving changes in skewness, we consider the fractional changes in low, high, and bulk variability. Fixing day of the year, denote the initial and final quantile difference as $\Delta q_{r,i}$ and $\Delta q_{r,f}$, where $r = l, m$, or h , indicated low tail, middle of the distribution (IQR) or high tail. The temporal change in quantile differences relative to the initial year is then

$$\rho = \frac{\Delta q_{r,f} - \Delta q_{r,i}}{\Delta q_{r,i}}. \quad (3)$$

Because we model the complete temperature distribution for each day of the year for all years, we choose representative days to understand winter and summer changes (Jan 1 and July 5, respectively), and consider the difference between the beginning and end of the scenarios, the years 1850 and 2000. For these representative days, we show in Figure 7 the fractional variability changes of ρ for low and high tails as well as the IQR.

Results show that tail changes can indeed differ strongly from changes in the bulk of the distribution. In wintertime (Figure 7, top row), in much of the northern mid-latitudes (including locations **a** and **b**), low tails change in a way that contributes to a more negative skew. Low tail variability contracts less than does the IQR, while high tail variability contracts more strongly. (High tails would contribute to more negative winter skew predominantly in the Hudson Bay region, where the model shows distinct bias.) In summertime (Figure 7, bottom row), the high tail dominates the transition to positive skew in the Southern Great Plains region (including location **c**).

To clarify the relative contributions of high and low tails to skewness changes, we also examine evolving temperature variability in the bulk and tails as a function of seasonality as well as long term change. Figure 8 shows absolute variability changes for the three example locations **a**, **b**, and **c** estimated using our quantile model, and for fractional changes see Supplementary Online

260 Material Figure S6. The uncertainty around our estimates is quantified by resampling the original
261 simulations (with replacement) and recomputing the estimates using this new set of simulations
262 (see Appendix A2c for details). In all locations, wintertime skewness changes are driven by the
263 relative changes in IQR and low tails. In the higher-latitude locations **a** and **b**, more negative winter
264 skew results because the IQR contracts even more strongly than does the low tail variability. In
265 the lower-latitude location **c**, more positive winter skew results because the IQR changes slightly
266 while the low tail variability contracts strongly.

267 The complexity of the relationships in Figure 8 also shows how misleading it may be to use a
268 three-month block to represent a season. While all three locations show larger IQR in winter than
269 summer, where the transition from winter to summer happens more quickly at some locations than
270 at others. This transition takes place abruptly in the northernmost location **a** and more gradually
271 in **c**. Low-tail variability seasonal transitions are even sharper than those of IQR in **a** and **b**, but
272 more gradual in **c**. In contrast, high-tail variability is more seasonally constant overall than low-
273 tail variability. Through these examples, we see how our method offers detailed information about
274 changes in variability across seasons and annual change, usually unavailable when analyzing each
275 season separately.

276 While we show only three locations in the text here, an online interactive application allows
277 similar in-depth examination of changes in model temperature distributions at all locations within
278 North America, available at <https://matzhaugen.com/links.html>. The application allows the user to
279 browse through any desired location to see how the variability changes as a function of season,
280 year and quantile difference. We include temperature histograms of the first and last simulation
281 year for the designated location, as well as maps that show the variability change spatially.

282 Another advantage of modeling quantiles as varying continuously from day to day and year to
283 year is that it makes it possible to estimate changes in the time of year that quantiles cross some

threshold temperature. To give an example, Figure 9 shows how the first day of the year on which various quantiles cross above -2.2°C and 0°C in the Detroit area (see Figure 9 where location **b** is analyzed). The cutoff of -2.2°C was selected because it was used in Pearse et al. (2017) as an indicator of the onset of Spring, although in that work it was the minimum temperature that was considered. The lower quantiles move earlier in the year more slowly than the 0.5 quantile, with the 0.25 quantile hitting the -2.2°C mark at a rate of approximately 15 days earlier per decade at present times. Note also that the 0.5 quantile never goes below the -2.2°C threshold after 2080, whereas, for the 0°C threshold, the median starts off in early March and moves up to late January by 2100. It is unclear how one would produce similar results using methods that segment average temperature into seasons.

5. Conclusions

We present a method to quantify changes in tail variability of temperature with high precision using a 50-member single climate model ensemble ((Srивer et al. 2015; Hogan and Srивer 2017; Vega-Westhoff and Srивer 2017)). Using data from the whole year and the whole span from 1850-2100 we estimate temperature quantiles as a function of seasonality and long term change. Analyzing the whole year simultaneously as opposed to analyzing each season separately allows for more flexible modeling of seasonality. Fitting these models stably can be achieved using large model ensembles sampling initial conditions uncertainty (i.e. internal variability).

By resampling entire simulations from the ensemble of climate simulations and recalculating the quantiles, we obtain confidence bands that do not require any assumptions of independence within any one simulation. We show that the smooth quantile estimates are accurate even across small intervals of the domain of the predictors. The fidelity of these intervals serves as a criterion to determine the required complexity in the statistical model.

307 The techniques presented in this study replicate several prior conclusions made in the literature,
308 e.g. the well-known projected decrease in winter variability in the northern mid-latitudes (e.g.
309 Schneider et al. 2015) most likely due to amplified warming in the arctic (Screen 2014). We
310 use differences between two quantiles in the same tail of the distribution as a tool for studying
311 more nuanced changes in distributions. Quantile regression makes it possible to give accurate
312 estimates of these quantiles that differ for every day and every year under study. Resampling
313 ensemble members yields confidence intervals for all quantities we estimate without having to
314 model temporal dependence within model runs. In the case study of CESM runs analyzed here,
315 we relate the changes in tail variability to changes in skewness of the temperature distributions,
316 and we find that in most of the domain analyzed, wintertime skewness changes are driven largely
317 by the relative behavior of IQR and low tails. For example, in much of the continental northern
318 U.S. and Canada, the low tail of temperature contracts substantially less than does the overall
319 temperature variability.

320 These results may inform physical explanations for the projection that skewness in winter tem-
321 perature changes in a dipole pattern across North America. It is possible that the skewness change
322 is a result of a change in the mean location and variability of the mid-latitude jet stream (e.g.
323 Barnes and Polvani 2013); this possibility may warrant further study.

324 The abundance of data available in large single model ensembles relative to single simulations
325 allows using quantile regression to accurately estimate high quantiles within a single model struc-
326 ture, avoiding some of the limitations of extreme value theory. Unlike quantile regression, methods
327 using extreme value theory require making assumptions about the shape of the tail of the distri-
328 bution. Of course, if one were interested in very extreme quantiles, say, below 0.001 or above
329 0.999, quantile regression estimates will become very noisy even with a 50-member ensemble,
330 and approaches using extreme value theory may become necessary.

331 By parameterizing the seasonally time-varying distribution of temperature through smooth func-
332 tions using the whole year as our domain, we reveal previously unavailable details about seasonal
333 transitions. For example, we show here that springtime variability decreases occur later in the year
334 at lower latitudes, and that seasonal transitions in tail variability differ from those in IQR. While
335 we analyze only temperature here, our method is intended to be general enough to be applied
336 to other climate variables such as precipitation or humidity. These detailed insights into climate
337 variable distributions may be valuable for risk assessment studies that emphasize extreme events.

338 **Acknowledgments**

339 This work was supported in part by STATMOS, the Research Network for Statistical Methods
340 for Atmospheric and Oceanic Sciences (NSF-DMS awards 1106862, 1106974 and 1107046), and
341 RDCEP, the University of Chicago Center for Robust Decision-making in Climate and Energy Pol-
342 icy (NSF grant SES-0951576). We acknowledge the University of Chicago Research Computing
343 Center, whose resources were used in the completion of this work. Ryan L. Sriver acknowledges
344 support from the Department of Energy sponsored Program on Integrated Assessment Model De-
345 velopment, Diagnostics and Inter-Model Comparisons (PIAMDDI), and the Program on Coupled
346 Human Earth Systems (PCHES).

A1. Model and reanalysis comparisons

Following the discussion on the paper, we define sample mean, variance and skewness as

$$\begin{aligned}\bar{x} &= \frac{1}{n} \sum_{i=1}^n x_i \\ s^2 &= \frac{1}{n} \sum_{i=1}^n (x_i - \bar{x})^2 \\ \gamma &= \frac{1}{n} \sum \left(\frac{x_i - \bar{x}}{s} \right)^3.\end{aligned}\tag{A1}$$

These definitions are used in Figures 2, 5, and 6 in the main text and in Supplementary Online Material Figures S1 and S2. We plot the standard deviation s rather than the variance s^2 .

A2. Model Details

In the following, we first give details regarding the regression of temperature quantiles on a fixed set of basis functions. We then discuss how to select the number of basis functions, through a “sufficiency criterion”. Lastly, we describe how we quantify uncertainty in the quantile estimates.

a. Model estimation

Given the number of basis functions in our model, represented by the columns in a matrix X with number of rows equal to the number of observations in the data set, we construct our temperature quantile estimate, \hat{T}_q , and corresponding coefficients, $\hat{\beta}_q$, viz.

$$\hat{T}_q = X\hat{\beta}_q\tag{A2}$$

such that the q^{th} fraction of residuals between the observations T at a particular location and their estimates, $T - \hat{T}_q$, are greater than zero and a fraction $1 - q$ are less than zero. With the

temperature model in Equation 2, our coefficient vector estimate, $\hat{\beta}$, contains the estimates of $\alpha, a_i, b_j, c_{i,j}$. Note that the seasonal interaction terms corresponding to the coefficients $c_{i,j}$ are not necessarily the same as the main seasonal terms corresponding to a_i . In fact, we find that fewer seasonal interaction terms are needed to describe the interaction behavior.

Computationally, obtaining the above quantile is equivalent to solving the following optimization problem (Koenker and Bassett Jr 1978),

$$\min_{\beta} \left\{ \sum_{d,t: T(d,t) \geq X(d,t)\beta} q|T(d,t) - X^T(d,t)\beta| + \sum_{d,t: T(d,t) < X(d,t)\beta} (1-q)|T(d,t) - X^T(d,t)\beta| \right\}, \quad (\text{A3})$$

and can be implemented in either R or MATLAB using existing libraries¹. Because we have access to 50 simulations, each location provides us with $365 \times 250 \times 50$ or approximately 4.5 million observations. Consequently, even fairly high quantiles can be accurately estimated without borrowing data from neighboring locations through a spatial model as done by e.g. Reich et al. (2011). However, making inferences about more extreme quantiles, such as the 0.001 or 0.999 quantiles, cannot be guaranteed to work as well with our methods.

We do not experience issues with quantile estimates crossing in our study area even though the optimization framework above does not explicitly enforce monotonicity with increasing quantile estimates. The absence of crossing quantiles is likely also due to the large sample size. For strict enforcement of monotonicity in the quantile curves see e.g. Bondell et al. (2010).

¹We use the R library `rq` and the function `rq.fit.pfn`, developed by Portnoy and Koenker (1997). Basis functions are created using `pbs` for periodic spline basis functions and `ns` for non-periodic splines. The non-periodic splines are constrained to be linear beyond the domain, 1850-2100, and are called *natural splines*.

378 *b. Model selection*

379 We describe our approach to selecting a modest set of basis functions that can accurately rep-
 380 resent the temperature data. If the model chosen has too many basis functions we run the risk of
 381 overfitting out-of-sample observations. To make sure this does not happen we need a metric to
 382 quantify the goodness-of-fit of the model.

383 Any reasonable temperature model we fit to the data will by definition contain the desired
 384 amount of positive and negative residuals *globally* according to the desired quantile q . A more
 385 stringent requirement would be that the smooth temperature estimate contains approximately an
 386 appropriate fraction of positive and negative residuals on a *daily* basis: for each d and t ,

$$S(d, t) = \frac{1}{n} \sum_{i=1}^n I [\hat{T}_i(d, t) - T_i(d, t) > 0] \approx q, \quad (\text{A4})$$

387 where I is the indicator function and n is the total number of samples (i.e. 50 for our CESM
 388 ensemble data set). If $S(d, t)$ is close to the value q for each d and t , the model would accurately
 389 describe the data and the number of basis functions is sufficient. In reality, we are looking basis
 390 functions that obey A4 with d averaged over blocks of days to increase the sample size, e.g. 10
 391 days blocks. It is also not the goal to capture the quantile at too short a timescale as events like
 392 volcanic eruptions would interfere with the estimate.

393 In order to estimate the appropriate number of basis functions, we hold out 5 simulations from
 394 the fitting process and use these to calculate our exceedences, which we call $S_{test}(d, t)$. We repeat
 395 this 10 times so that all the simulations are eventually held out, giving 10 samples of $S_{test}(d, t)$. As
 396 we increase model complexity through degrees of freedom in the basis functions, the variability
 397 of S_{test} should reach a minimum when the necessary number of basis functions is reached and
 398 the quantile estimate is the same for each time point. If the number of basis functions is increased
 399 beyond this point, we start to overfit the data and the out-of-sample variability of S_{test} will increase.

400 To estimate S_{test} , we block the variables in two ways, one for each variable. First, we divide
 401 each year in 10-day bins and calculate the average exceedence estimate, \hat{S}_{test} , in each bin. We
 402 sum over the whole domain of long term change, t , and a subset of the seasonality variable, d .
 403 Specifically, let A be a set of non-overlapping contiguous blocks of days that together cover the
 404 whole year, where a_j , $j = 1, \dots, m$ are the elements of the set. Also let T be the index set for
 405 long term change, $T = [1850, 2100]$, measured in years. Then, for all $a_j \in A$,

$$\hat{S}_{test}(a_j) = \frac{1}{n} \sum_{i=[1,n], d \in a_j, t \in T} I[\hat{T}_i(d, t) - T_i(d, t) > 0]. \quad (A5)$$

406 To get an equal number of days in each bin we use the first 360 days of the year only.

407 Second, we divide the long term change variable, t , in bins and repeat the process by flipping the
 408 role of the variables in Equation A5 to get a set of $\hat{S}_{test}(b_j)$ with $b_j \in B$, a set of non-overlapping
 409 contiguous blocks of long-term change indices in T . An example of the blocked exceedence
 410 estimate is shown in Figure 10. Note that the pointwise quantile estimate is contained between
 411 the error bars, suggesting that the model is sufficiently complex. The standard deviation of these
 412 estimates of \hat{S}_{test} is our measure of exceedence variability.

413 We seek the simplest model that gives good calibration of the quantile estimates (so close to 0.05
 414 in Figure 10). At the same time we have to watch out to not overfit the data so we also want to
 415 minimize out-of-sample variability. We find that a model with 15 seasonal, 3 seasonal-interaction
 416 and 4 temporal degrees of freedom minimizes the variability of exceedences \hat{S}_{test} , shown in Figure
 417 11, where seasonality has been binned. The out-of-sample fit when binning long-term change is
 418 shown in Figure S7 in the supplement. Here, models 4-6 have approximately equal test error, so
 419 since binning seasonality suggests the complexity of model 6, we chose model 6 as the overall
 420 model. Including the possible interaction terms, the full model has 32 free parameters to be fitted,

421 or $\hat{\beta} \in \mathbb{R}^{32}$. All model candidates are shown in Table 1. We reach the same conclusion when
422 blocking the long term change, t , and when analyzing different spatial locations (see Figure S7).

423 *c. Uncertainty Estimation*

424 With a reasonable model chosen through cross-validation, we present a way to quantify its uncer-
425 tainty. Because we are using multiple simulations that are assumed independent, we resample en-
426 tire simulations from the set of 50 simulations. Resampling 50 new simulations with replacement
427 from the original set of simulations yields a new dataset. From the new data set we obtain another
428 temperature estimate with the same model basis functions but different coefficients, β^* . After re-
429 peating this resampling and re-estimating procedure 100 times we generate pointwise confidence
430 intervals for temperature quantiles. For example, in Figure 8 we show the 90% confidence interval
431 by selecting the pointwise .05 and .95 quantiles of temperature variability estimates. Because the
432 confidence intervals are quite tight we deem the 100 new estimates (or bootstraps) sufficient to
433 indicate that the results we describe in section 4 are not due to random variation. Larger number
434 of bootstrap replicates might give slightly more accurate intervals but would not change our con-
435 clusions. One might also consider fewer simulations as a compromise between computation time
436 and quality of the estimates. Assuming normally distributed confidence intervals, we would expect
437 the standard error to scale as $1/\sqrt{n}$. Thus, if one is willing to widen the confidence intervals by
438 a factor of 2 (approximately) only 10 simulations would suffice. However, one could compensate
439 for this greater variability by using fewer basis functions at a cost, of course, of obtaining less
440 resolved estimates of seasonal patterns and long-term trends in the quantiles.

References

- Barnes, E. A., and L. Polvani, 2013: Response of the midlatitude jets, and of their variability, to increased greenhouse gases in the CMIP5 models. *Journal of Climate*, **26** (18), 7117–7135.
- Bondell, H. D., B. J. Reich, and H. Wang, 2010: Noncrossing quantile regression curve estimation. *Biometrika*, **97** (4), 825–838.
- Chapman, S. C., D. A. Stainforth, and N. W. Watkins, 2013: On estimating local long-term climate trends. *Phil. Trans. R. Soc. A*, **371** (1991), 20120287.
- Chavez-Demoulin, V., and A. C. Davison, 2005: Generalized additive modelling of sample extremes. *Journal of the Royal Statistical Society: Series C (Applied Statistics)*, **54** (1), 207–222.
- Davison, A. C., S. A. Padoan, and M. Ribatet, 2012: Statistical modeling of spatial extremes. *Statistical science*, 161–186.
- Davison, A. C., and R. L. Smith, 1990: Models for exceedances over high thresholds. *Journal of the Royal Statistical Society. Series B (Methodological)*, 393–442.
- Dee, D. P., and Coauthors, 2011: The ERA-interim reanalysis: Configuration and performance of the data assimilation system. *Quarterly Journal of the royal meteorological society*, **137** (656), 553–597.
- Deser, C., R. Knutti, S. Solomon, and A. S. Phillips, 2012a: Communication of the role of natural variability in future North American climate. *Nature Climate Change*, **2** (11), 775–779.
- Deser, C., A. Phillips, V. Bourdette, and H. Teng, 2012b: Uncertainty in climate change projections: the role of internal variability. *Climate Dynamics*, **38** (3-4), 527–546.

Deser, C., A. S. Phillips, M. A. Alexander, and B. V. Smoliak, 2014: Projecting North American climate over the next 50 years: Uncertainty due to internal variability. *Journal of Climate*, **27** (6), 2271–2296.

Diffenbaugh, N. S., D. L. Swain, and D. Touma, 2015: Anthropogenic warming has increased drought risk in California. *Proceedings of the National Academy of Sciences*, **112** (13), 3931–3936.

Donat, M. G., and L. V. Alexander, 2012: The shifting probability distribution of global daytime and night-time temperatures. *Geophysical Research Letters*, **39** (14).

Eastoe, E. F., and J. A. Tawn, 2009: Modelling non-stationary extremes with application to surface level ozone. *Journal of the Royal Statistical Society: Series C (Applied Statistics)*, **58** (1), 25–45.

Fischer, E. M., and R. Knutti, 2014: Detection of spatially aggregated changes in temperature and precipitation extremes. *Geophysical Research Letters*, **41** (2), 547–554.

Franzke, C. L., 2015: Local trend disparities of european minimum and maximum temperature extremes. *Geophysical Research Letters*, **42** (15), 6479–6484.

Gao, M., and C. L. Franzke, 2017: Quantile regression–based spatiotemporal analysis of extreme temperature change in china. *Journal of Climate*, **30** (24), 9897–9914.

Hagos, S. M., L. R. Leung, J.-H. Yoon, J. Lu, and Y. Gao, 2016: A projection of changes in landfalling atmospheric river frequency and extreme precipitation over western North America from the Large Ensemble CESM simulations. *Geophysical Research Letters*.

Hastie, T., R. Tibshirani, and J. Friedman, 2009: *Elements of Statistical Learning*. 2nd ed., Springer.

482 Hogan, E., and R. Sriver, 2017: Analyzing the effect of ocean internal variability on depth-
483 integrated steric sea-level rise trends using a low-resolution cesm ensemble. *Water*, **9** (7), 483.

484 Huang, W. K., M. L. Stein, D. J. McInerney, S. Sun, and E. J. Moyer, 2015a: Changes in US tem-
485 perature extremes under increased CO2 in millennial-scale climate simulations. *arXiv preprint*
486 *arXiv:1512.08775*.

487 Huang, W. K., M. L. Stein, D. J. McInerney, S. Sun, and E. J. Moyer, 2015b: Estimating changes
488 in temperature extremes from millennial scale climate simulations using generalized extreme
489 value (GEV) distributions. *arXiv preprint arXiv:1512.08775*.

490 Huser, R., and A. Davison, 2014: Space–time modelling of extreme events. *Journal of the Royal*
491 *Statistical Society: Series B (Statistical Methodology)*, **76** (2), 439–461.

492 Huybers, P., K. A. McKinnon, A. Rhines, and M. Tingley, 2014: US daily temperatures: The
493 meaning of extremes in the context of nonnormality. *Journal of Climate*, **27** (19), 7368–7384.

494 Jalbert, J., A.-C. Favre, C. Bélisle, and J.-F. Angers, 2017: A spatiotemporal model for extreme
495 precipitation simulated by a climate model, with an application to assessing changes in return
496 levels over North America. *Journal of the Royal Statistical Society: Series C (Applied Statistics)*.

497 Katz, R. W., and B. G. Brown, 1992: Extreme events in a changing climate: variability is more
498 important than averages. *Climatic change*, **21** (3), 289–302.

499 Kay, J. E., and Coauthors, 2015: The Community Earth System Model (CESM) large ensemble
500 project: A community resource for studying climate change in the presence of internal climate
501 variability. *Bulletin of the American Meteorological Society*, **96** (8), 1333–1349.

502 Kitoh, A., and T. Mukano, 2009: Changes in daily and monthly surface air temperature variability
 503 by multi-model global warming experiments. *Journal of the Meteorological Society of Japan.*
 504 *Ser. II*, **87 (3)**, 513–524.

505 Koenker, R., and G. Bassett Jr, 1978: Regression quantiles. *Econometrica: journal of the Econo-*
 506 *metric Society*, 33–50.

507 McKinnon, K. A., A. Rhines, M. P. Tingley, and P. Huybers, 2016: The changing shape of northern
 508 hemisphere summer temperature distributions. *Journal of Geophysical Research: Atmospheres*,
 509 **121 (15)**, 8849–8868.

510 Meehl, G. A., C. Tebaldi, G. Walton, D. Easterling, and L. McDaniel, 2009: Relative increase of
 511 record high maximum temperatures compared to record low minimum temperatures in the US.
 512 *Geophysical Research Letters*, **36 (23)**.

513 Moss, R. H., and Coauthors, 2010: The next generation of scenarios for climate change research
 514 and assessment. *Nature*, **463 (7282)**, 747–756.

515 Northrop, P. J., and P. Jonathan, 2011: Threshold modelling of spatially dependent non-stationary
 516 extremes with application to hurricane-induced wave heights. *Environmetrics*, **22 (7)**, 799–809.

517 Otto, F. E. L., N. Massey, G. J. Oldenborgh, R. G. Jones, and M. R. Allen, 2012: Reconciling two
 518 approaches to attribution of the 2010 Russian heat wave. *Geophysical Research Letters*, **39 (4)**.

519 Pearse, W. D., C. C. Davis, D. W. Inouye, R. B. Primack, and T. J. Davies, 2017: A statistical
 520 estimator for determining the limits of contemporary and historic phenology. *Nature ecology &*
 521 *evolution*, **1 (12)**, 1876.

522 Poppick, A., E. J. Moyer, and M. L. Stein, 2017: Estimating trends in the global mean temperature
523 record. *Advances in Statistical Climatology, Meteorology and Oceanography*, **3** (1), 33–53, doi:
524 10.5194/ascmo-3-33-2017, URL <http://www.adv-stat-clim-meteorol-oceanogr.net/3/33/2017/>.

525 Portnoy, S., and R. Koenker, 1997: The Gaussian hare and the laplacian tortoise: computability of
526 squared-error versus absolute-error estimators. *Statistical Science*, **12** (4), 279–300.

527 Räisänen, J., 2002: CO₂-induced changes in interannual temperature and precipitation variability
528 in 19 CMIP2 experiments. *Journal of Climate*, **15** (17), 2395–2411.

529 Reich, B. J., M. Fuentes, and D. B. Dunson, 2011: Bayesian spatial quantile regression. *Journal*
530 *of the American Statistical Association*, **106** (493), 6–20.

531 Rhines, A., K. A. McKinnon, M. P. Tingley, and P. Huybers, 2017: Seasonally resolved distribu-
532 tional trends of North American temperatures show contraction of winter variability. *Journal of*
533 *Climate*, **30** (3), 1139–1157.

534 Rodgers, K. B., J. Lin, and T. L. Frölicher, 2015: Emergence of multiple ocean ecosystem drivers
535 in a large ensemble suite with an Earth System Model. *Biogeosciences*, **12** (11), 3301.

536 Schneider, T., T. Bischoff, and H. Plotka, 2015: Physics of changes in synoptic midlatitude tem-
537 perature variability. *Journal of Climate*, **28** (6), 2312–2331.

538 Screen, J. A., 2014: Arctic amplification decreases temperature variance in northern mid-to high-
539 latitudes. *Nature Climate Change*, **4** (7), 577–582.

540 Semenov, V., and L. Bengtsson, 2002: Secular trends in daily precipitation characteristics: green-
541 house gas simulation with a coupled AOGCM. *Climate Dynamics*, **19** (2), 123–140.

542 Shields, C. A., D. A. Bailey, G. Danabasoglu, M. Jochum, J. T. Kiehl, S. Levis, and S. Park, 2012:
543 The low-resolution CCSM4. *Journal of Climate*, **25** (12), 3993–4014.

544 Singh, D., and Coauthors, 2014: Severe precipitation in Northern India in June 2013: causes,
 545 historical context, and changes in probability. *Bulletin of the American Meteorological Society*,
 546 **95 (9)**, S58.

547 Smith, R., and Coauthors, 2010: The parallel ocean program (POP) reference manual ocean com-
 548 ponent of the Community Climate system Model (ccsm) and Community Earth System Model
 549 (CESM). *Rep. LAUR-01853*, **141**.

550 Srivier, R. L., C. E. Forest, and K. Keller, 2015: Effects of initial conditions uncertainty on regional
 551 climate variability: An analysis using a low-resolution CESM ensemble. *Geophysical Research*
 552 *Letters*, **42 (13)**, 5468–5476.

553 Stainforth, D. A., S. C. Chapman, and N. W. Watkins, 2013: Mapping climate change in European
 554 temperature distributions. *Environmental Research Letters*, **8 (3)**, 034 031.

555 Stott, P. A., D. A. Stone, and M. R. Allen, 2004: Human contribution to the European heatwave
 556 of 2003. *Nature*, **432 (7017)**, 610–614.

557 Swain, D. L., M. Tsang, M. Haugen, D. Singh, A. Charland, B. Rajaratnam, and N. S. Diffen-
 558 baugh, 2014: The extraordinary California drought of 2013/2014: Character, context, and the
 559 role of climate change. *Bulletin of the American Meteorological Society*, **95 (9)**, S3.

560 Thompson, D. W. J., E. A. Barnes, C. Deser, W. E. Foust, and A. S. Phillips, 2015: Quantifying
 561 the role of internal climate variability in future climate trends. *Journal of Climate*, **28 (16)**,
 562 6443–6456.

563 Trenberth, K. E., 2011: Attribution of climate variations and trends to human influences and
 564 natural variability. *Wiley Interdisciplinary Reviews: Climate Change*, **2 (6)**, 925–930.

- 565 Trenberth, K. E., J. T. Fasullo, and T. G. Shepherd, 2015: Attribution of climate extreme events.
566 *Nature Climate Change*, **5** (8), 725–730.
- 567 Vega-Westhoff, B., and R. L. Sriver, 2017: Analysis of ensos response to unforced variability and
568 anthropogenic forcing using cesm. *Scientific reports*, **7** (1), 18 047.

569 **LIST OF TABLES**

570	Table 1.	Degrees of freedom in the spline basis for each independent variable, with the	
571		interaction terms including the reduced set of seasonal polynomials with de-	
572		grees of freedom listed in the middle column. The temporal polynomials are	
573		the same in both the main and interaction terms.	30

	Seasonal	Seasonal-Int.	Temporal
1	5	3	3
2	7	3	3
3	10	3	3
4	10	3	4
5	12	3	4
6	15	3	4
7	15	3	5
8	15	5	5
9	18	5	5

TABLE 1. Degrees of freedom in the spline basis for each independent variable, with the interaction terms including the reduced set of seasonal polynomials with degrees of freedom listed in the middle column. The temporal polynomials are the same in both the main and interaction terms.

LIST OF FIGURES

- 578 **Fig. 1.** An illustration of concepts and values related to distributions used in this paper. The cartoon shows a
 579 positively skewed (or “right-skewed”) probability distribution and the three quantile differences discussed
 580 in this paper, in the low tail, high tail, and middle of the distribution. The q quantile in a distribution is the
 581 value such that the probability of being below it has probability q . Here Δq_l is the difference between the
 582 0.05 and 0.025 quantiles; the IQR or Interquartile Range that between the 0.75 and 0.25 quantiles; and Δq_h
 583 that between the 0.975 and 0.95 quantiles. The values Δq_l and Δq_h quantify variability in extreme values
 584 while IQR quantifies variability in the bulk of the distribution. 33
- 585 **Fig. 2.** Comparison of daily temperature distribution properties (mean, standard deviation, and skewness) between
 586 the CESM ensemble and ERA-Interim, for winter (DJF; aggregating all daily temperatures without deseasonalizing). We compare the years 1979-1994, the first available 15 years of the ERA-Interim dataset, and
 587 upscale the reanalysis from 0.75° to 3.75° resolution to match CESM. Units on top two rows are degrees
 588 Celsius; bottom row showing skewness is dimensionless. Winter skewness over the continental U.S. is neg-
 589 ative in both model and reanalysis, implying a thicker lower tail; see Figure 1 and Appendix A1 for example
 590 and definitions. Overall, large-scale geospatial patterns are similar in both data sets, though some discrep-
 591 ancies are present (e.g. abnormally cold model Arctic winters). Letters **a-c** mark locations that will be used
 592 in examples throughout the paper; these are ordered from north to south, with latitudes and longitudes **a**
 593 (50.1, -101), **b** (42.7, -82), **c** (35.3, -98). 34
- 595 **Fig. 3.** Illustration of results of our quantile estimation procedure using the 50-member CESM ensemble. The
 596 figure shows ensemble daily mean temperatures for the year 1850 for the three representative locations **a**, **b**,
 597 and **c** defined in Figure 2. The ensemble provides 50 points per day but for clarity we show only 10% of the
 598 data. Solid lines show the median daily temperature and dashed lines the .025 and .975 quantiles estimated
 599 by our procedure. (Note the higher variabilities in winter.) Note that the location of the points exceeding
 600 the smooth median estimate are approximately uniform across time (notwithstanding the amplitudes of
 601 residuals), suggesting that the quantile estimate is accurate for each day. XX put in Michael’s text here
 602 At all sites, the estimated quantile curves capture the seasonally changing patterns in the distributions
 603 reasonably well. 35
- 604 **Fig. 4.** Evolving distributions of daily mean temperature in the CESM ensemble RCP8.5 model runs at the loca-
 605 tions **a**, **b**, **c** defined in Figure 2. Each distribution includes temperatures from a 15-day period over 15
 606 model years for a total of 11,250 observations (15 days \times 15 years \times 50 ensemble members). Winter distri-
 607 butions are taken from Jan 1-15 and summer July 5-19; “initial” distributions include years 1850-1864 and
 608 “final” years 2096-2100. Changes in distributions are readily apparent, especially in winter at higher lati-
 609 tudes (locations **a** and **b**), but detailed quantification, especially of tail changes, requires more sophisticated
 610 techniques. 36
- 611 **Fig. 5.** Initial temperature distribution properties (left) and their changes over time (right) in the CESM ensemble
 612 RCP8.5 model runs, for aggregate wintertime (DJF) daily temperature. Initial (“pre-industrial”) and final
 613 periods are defined as in Figure 4, as 15-year periods 1850–1864 and 2086–2100. Distributional moments
 614 (mean, standard deviation, and skewness) are defined as in Figure 2. Units on the top two rows are degrees
 615 Celsius, while the bottom row showing skewness is dimensionless. Gray crosses mark locations where
 616 the changes are not significant at the 0.05 level, obtained by resampling the set of 50 simulations (with
 617 replacement) and recalculating the sample moments. *Top right:* Mean temperature universally increases.
 618 Extreme warming in the Hudson’s Bay region occurs where the model is biased low in present-day simu-
 619 lations. *Middle right:* As expected, standard deviation decreases strongly at higher latitudes. *Bottom right:*
 620 Changes in winter skewness show a dipole pattern, which enhances negative skew above $\sim 40^\circ$ but reduces
 621 it at lower latitudes. 37
- 622 **Fig. 6.** As in Figure 5 but for aggregate summer (JJA) temperatures, and note that scales differ from those in Figure
 623 5. Except in the desert Southwest and Mexico, changes in standard deviation (*middle right*) and skewness
 624 (*bottom right*) are generally smaller in summer than in winter and often not significant at the 0.05 level. 38
- 625 **Fig. 7.** Changes in daily temperature variability (quantile differences) over time in CESM ensemble RCP8.5 runs
 626 estimated using our statistical approach. Because our approach removes the need to aggregate over time

when presenting changes, we show here differences in distributions for a single day and year: Jan 1 for winter (*top*) and July 5 for summer (*bottom*), with differences evaluated between the years 1850 and 2100. Changes are expressed as fractions of initial variability (see (3) for definition), so that the value 0 indicates no change with respect to the initial year. *Left*, *middle*, and *right* columns show, respectively, changes in low tail variability, IQR, and high tail variability, as previously defined. Gray crosses mark grid points where the change is less than 3 standard deviations from the original estimate. As expected, estimated changes in IQR (*middle*) are similar to changes in standard deviation seen in Figures 5 and 6. Changes in tail variability are clearly different from those in IQR, meaning that future distributions are not simply a rescaling of the present-day distributions. 39

Fig. 8. Evolving daily temperature variability (quantile differences) over time in CESM ensemble RCP8.5 runs estimated using our statistical approach, for locations **a**, **b**, and **c**. Using the analysis described in Figure 7, we show absolute IQR and tail variability as a function of seasonality, with different years (at 40 year intervals) shown as different colored lines, from 1850 (dark blue) to 2090 (dark red). Dashed lines represent pointwise 90% confidence intervals. Note the complexity of seasonal cycles in variability at different locations. These results show that the dipole pattern of changes in wintertime skewness changes seen in Figure 5 is driven by low rather than high tail behavior. In wintertime, in the more northern locations **a** and **b**, IQR reduces more strongly than does low tail variability, making skew more negative. In the more southern location **c**, IQR change is negligible while low tail variability reduces strongly, making skew more positive. In all locations, absolute changes in wintertime low tail variability are larger than changes in high tails. For fractional changes, see Supplementary Online Material Figure S6. 40

Fig. 9. First day above freezing (solid lines) and -2.2°C (dashed lines) for each year from 1850-2100 as measured by fitting quantiles to average daily temperature of the CESM ensemble data set. Three quantiles are shown to capture the spread of the distribution, 0.5 (green), 0.25 (red) and 0.05 (black). 41

Fig. 10. Exceedence probability of temperature events above the .95 quantile estimate. The density is obtained by making 10-day bins and counting the number of observations that are above the quantile estimate and normalizing by the total number of exceedences aggregated across all model runs. Each bin is represented by the bin start day, i.e. an x-axis value of 0 includes the interval $(0, 10]$. We hold out 10 different sets of simulations to obtain 10 different estimates for each block of time, from which we calculate their mean shown as points and standard deviation shown as error bars around \hat{S}_{test} 42

Fig. 11. Training and test exceedence standard deviation as a function of model number, where increasing model number signifies increasing degrees of freedom in the spline basis functions. The data were extracted from the gridbox located at $(\text{lat}, \text{lon}) = (31.5, -93.8)$. The exceedence is calculated by binning seasonality in 10-day blocks and summing over the long term change. 43

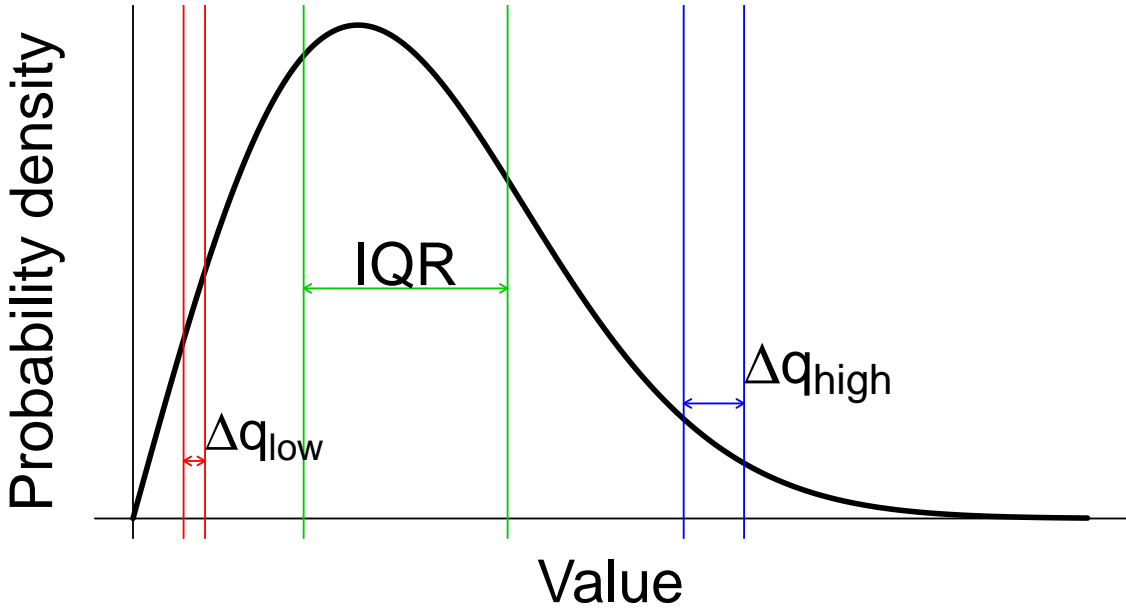


FIG. 1. An illustration of concepts and values related to distributions used in this paper. The cartoon shows a positively skewed (or “right-skewed”) probability distribution and the three quantile differences discussed in this paper, in the low tail, high tail, and middle of the distribution. The q quantile in a distribution is the value such that the probability of being below it has probability q . Here Δq_l is the difference between the 0.05 and 0.025 quantiles; the IQR or Interquartile Range that between the 0.75 and 0.25 quantiles; and Δq_h that between the 0.975 and 0.95 quantiles. The values Δq_l and Δq_h quantify variability in extreme values while IQR quantifies variability in the bulk of the distribution.

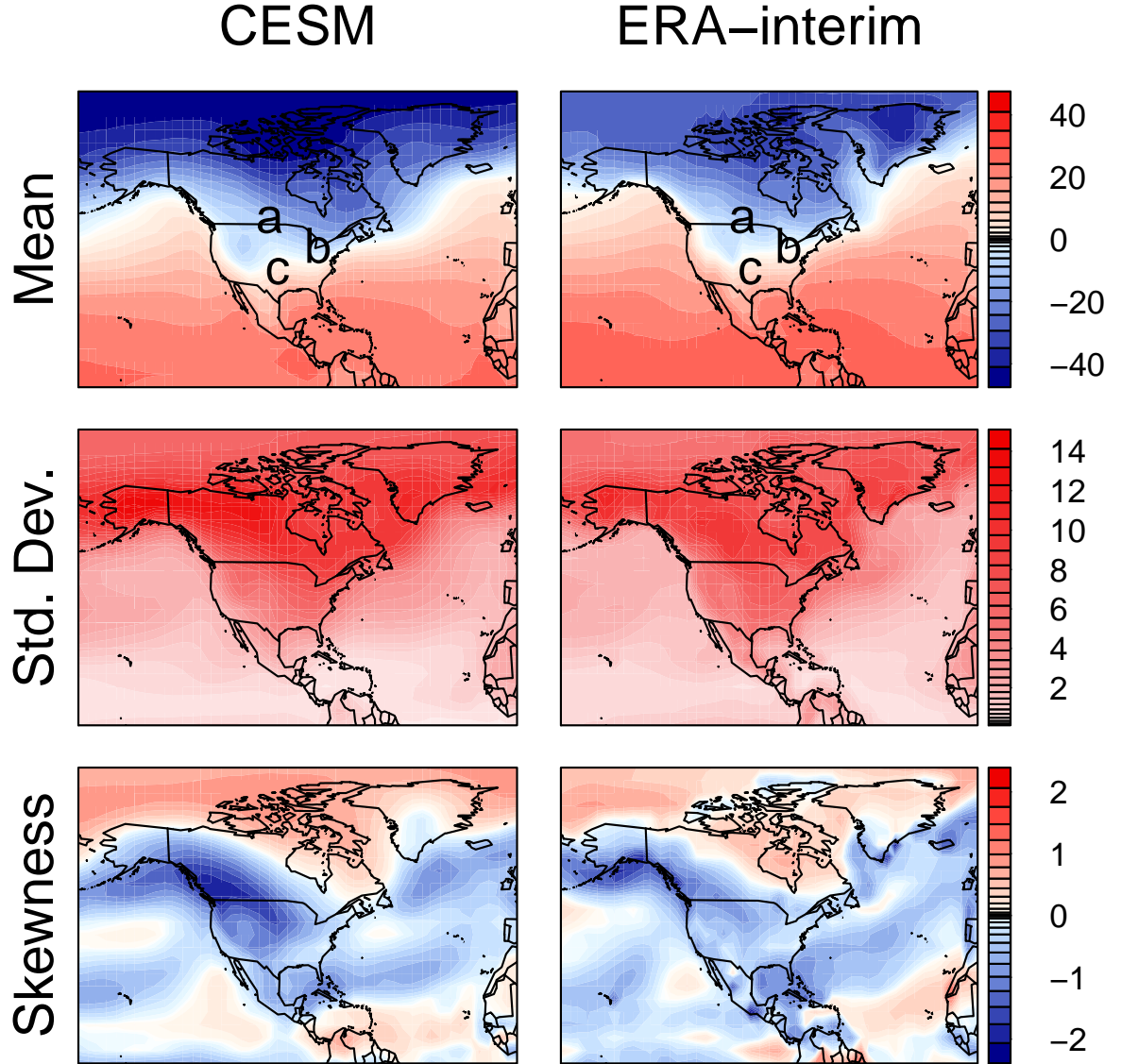
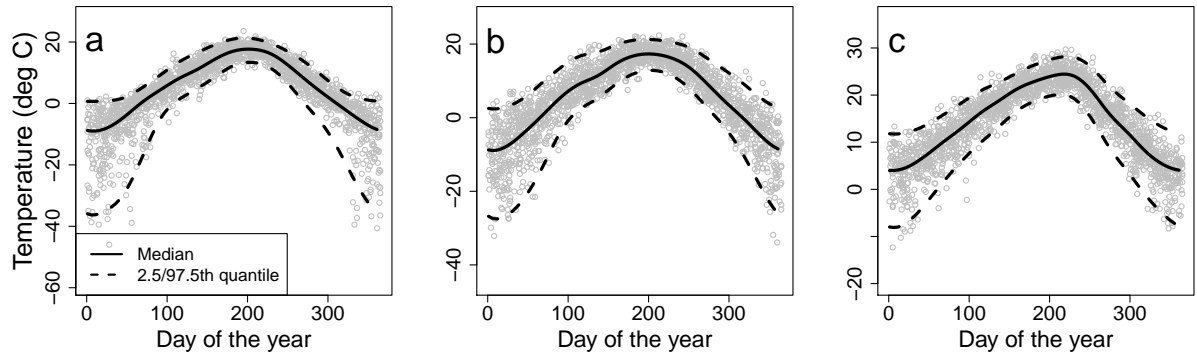


FIG. 2. Comparison of daily temperature distribution properties (mean, standard deviation, and skewness) between the CESM ensemble and ERA-Interim, for winter (DJF; aggregating all daily temperatures without deseasonalizing). We compare the years 1979-1994, the first available 15 years of the ERA-Interim dataset, and upscale the reanalysis from 0.75° to 3.75° resolution to match CESM. Units on top two rows are degrees Celsius; bottom row showing skewness is dimensionless. Winter skewness over the continental U.S. is negative in both model and reanalysis, implying a thicker lower tail; see Figure 1 and Appendix A1 for example and definitions. Overall, large-scale geospatial patterns are similar in both data sets, though some discrepancies are present (e.g. abnormally cold model Arctic winters). Letters **a-c** mark locations that will be used in examples throughout the paper; these are ordered from north to south, with latitudes and longitudes **a** (50.1, -101), **b** (42.7, -82), **c** (35.3, -98).



674 FIG. 3. Illustration of results of our quantile estimation procedure using the 50-member CESM ensemble. The figure shows
 675 ensemble daily mean temperatures for the year 1850 for the three representative locations **a**, **b**, and **c** defined in Figure 2. The
 676 ensemble provides 50 points per day but for clarity we show only 10% of the data. Solid lines show the median daily temperature
 677 and dashed lines the .025 and .975 quantiles estimated by our procedure. (Note the higher variabilities in winter.) Note that
 678 the location of the points exceeding the smooth median estimate are approximately uniform across time (notwithstanding the
 679 amplitudes of residuals), suggesting that the quantile estimate is accurate for each day. XX put in Michael's text here At all sites,
 680 the estimated quantile curves capture the seasonally changing patterns in the distributions reasonably well.

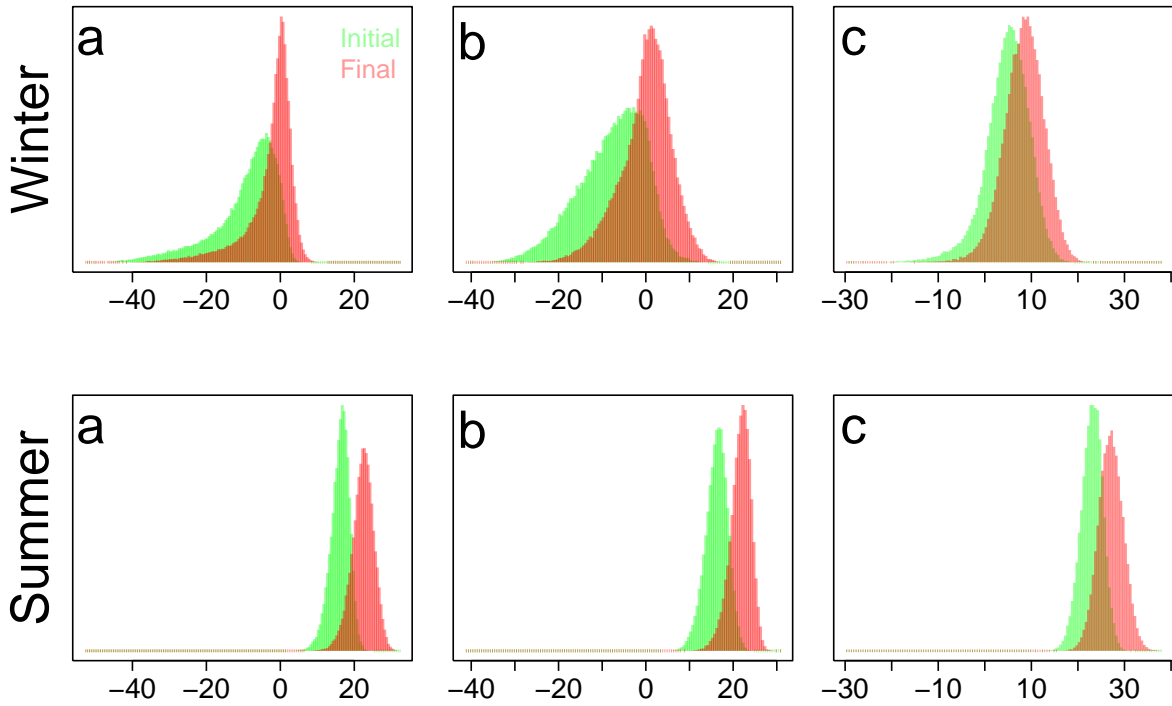


FIG. 4. Evolving distributions of daily mean temperature in the CESM ensemble RCP8.5 model runs at the locations **a**, **b**, **c** defined in Figure 2. Each distribution includes temperatures from a 15-day period over 15 model years for a total of 11,250 observations (15 days \times 15 years \times 50 ensemble members). Winter distributions are taken from Jan 1-15 and summer July 5-19; “initial” distributions include years 1850-1864 and “final” years 2096-2100. Changes in distributions are readily apparent, especially in winter at higher latitudes (locations **a** and **b**), but detailed quantification, especially of tail changes, requires more sophisticated techniques.

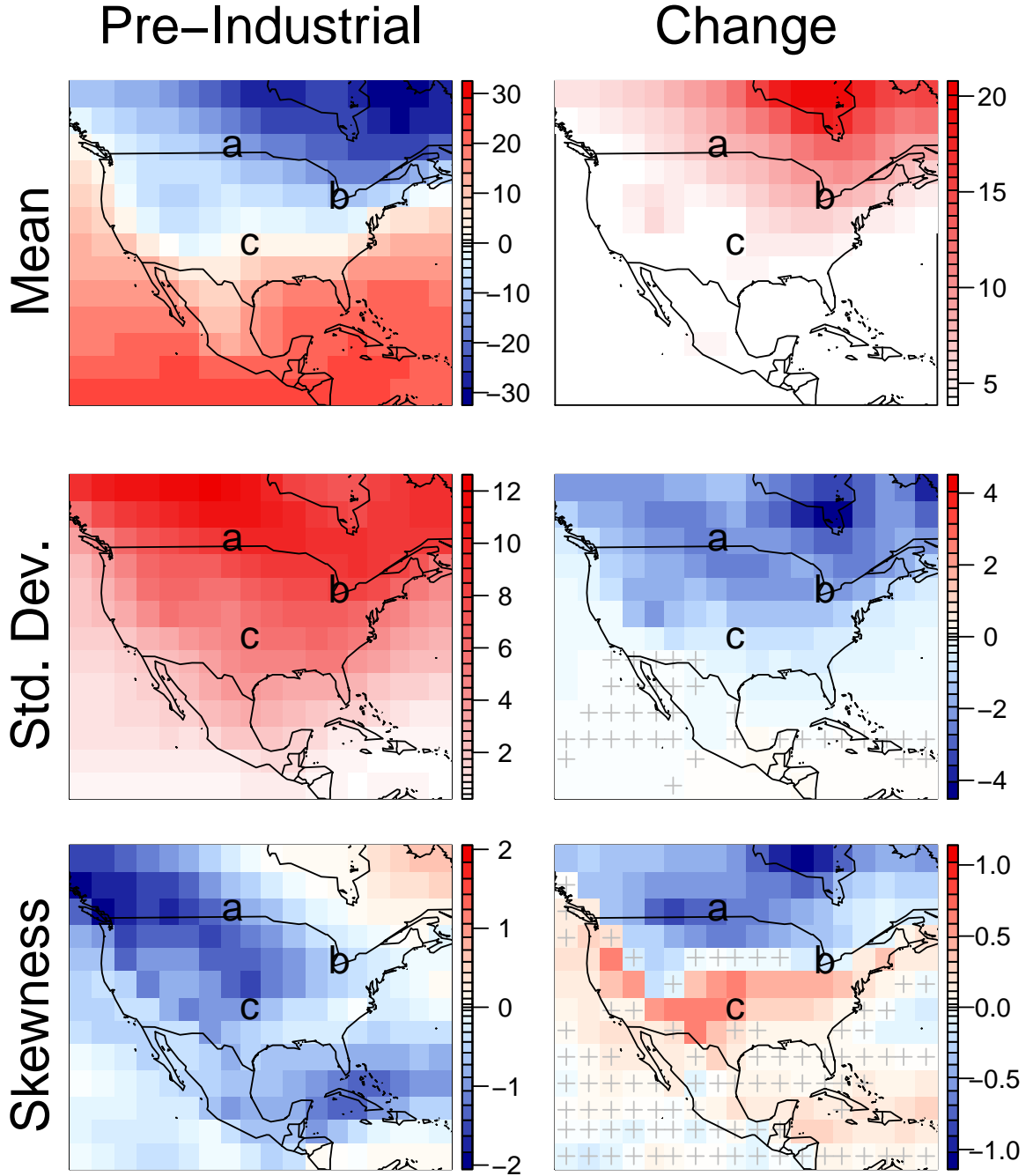


FIG. 5. Initial temperature distribution properties (left) and their changes over time (right) in the CESM ensemble RCP8.5 model runs, for aggregate wintertime (DJF) daily temperature. Initial (“pre-industrial”) and final periods are defined as in Figure 4, as 15-year periods 1850–1864 and 2086–2100. Distributional moments (mean, standard deviation, and skewness) are defined as in Figure 2. Units on the top two rows are degrees Celsius, while the bottom row showing skewness is dimensionless. Gray crosses mark locations where the changes are not significant at the 0.05 level, obtained by resampling the set of 50 simulations (with replacement) and recalculating the sample moments. *Top right:* Mean temperature universally increases. Extreme warming in the Hudson’s Bay region occurs where the model is biased low in present-day simulations. *Middle right:* As expected, standard deviation decreases strongly at higher latitudes. *Bottom right:* Changes in winter skewness show a dipole pattern, which enhances negative skew above $\sim 40^\circ$ but reduces it at lower latitudes.

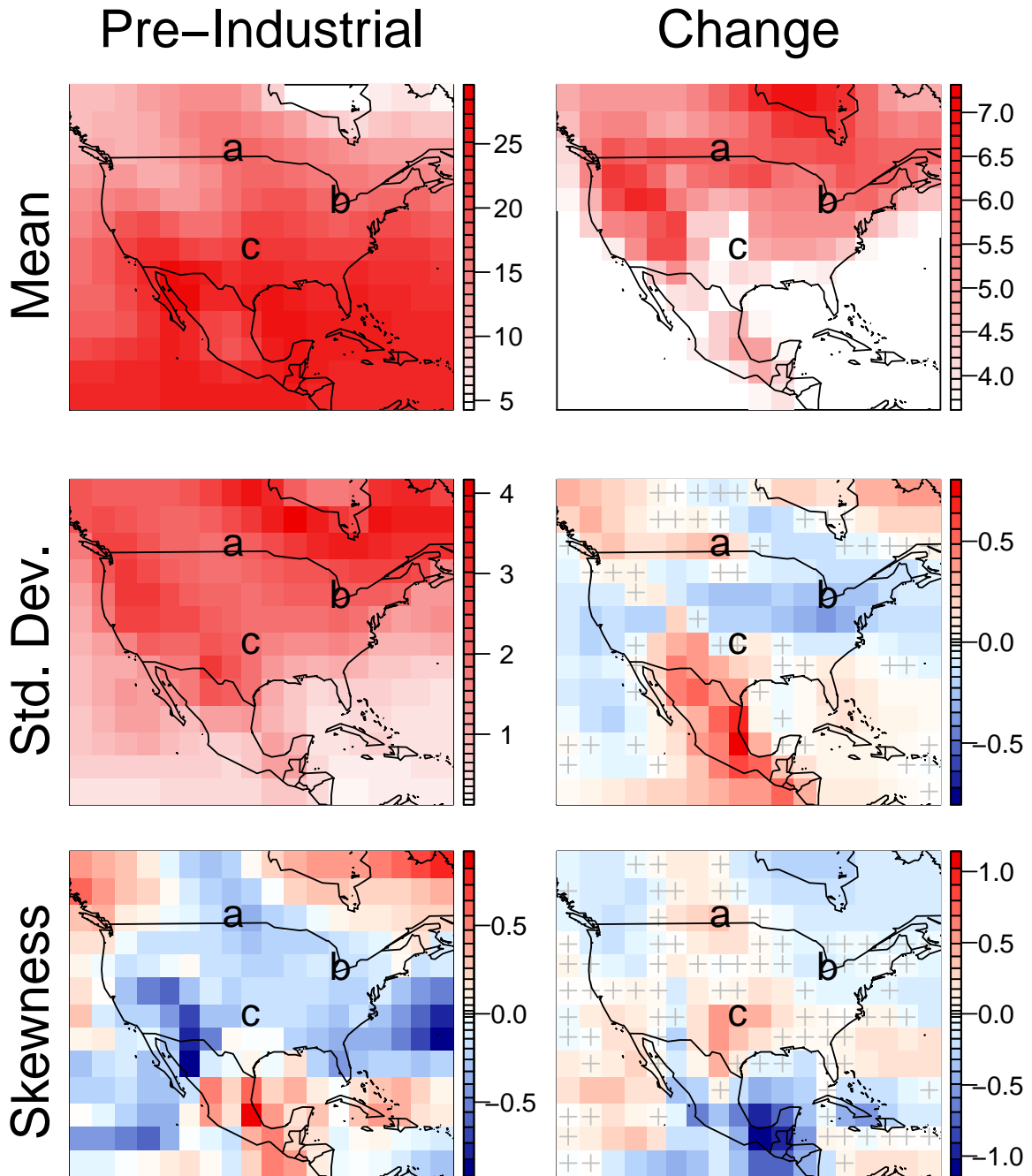


FIG. 6. As in Figure 5 but for aggregate summer (JJA) temperatures, and note that scales differ from those in Figure 5. Except in the desert Southwest and Mexico, changes in standard deviation (*middle right*) and skewness (*bottom right*) are generally smaller in summer than in winter and often not significant at the 0.05 level.

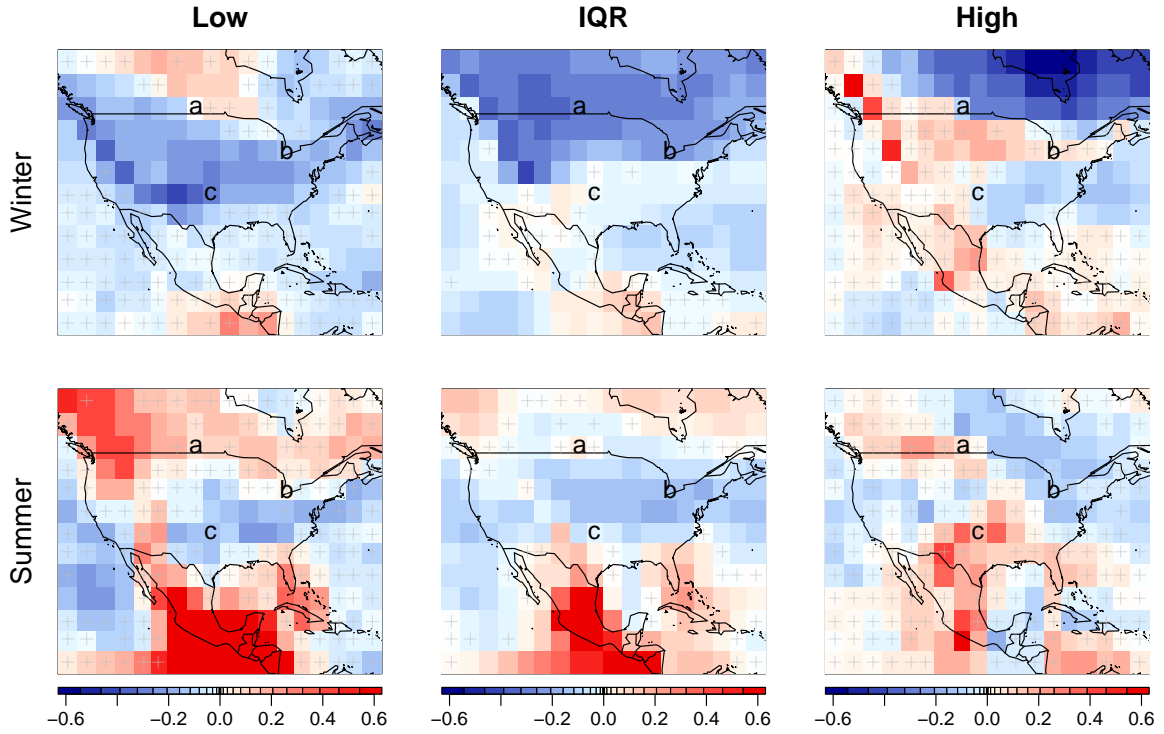


FIG. 7. Changes in daily temperature variability (quantile differences) over time in CESM ensemble RCP8.5 runs estimated using our statistical approach. Because our approach removes the need to aggregate over time when presenting changes, we show here differences in distributions for a single day and year: Jan 1 for winter (*top*) and July 5 for summer (*bottom*), with differences evaluated between the years 1850 and 2100. Changes are expressed as fractions of initial variability (see (3) for definition), so that the value 0 indicates no change with respect to the initial year. *Left*, *middle*, and *right* columns show, respectively, changes in low tail variability, IQR, and high tail variability, as previously defined. Gray crosses mark grid points where the change is less than 3 standard deviations from the original estimate. As expected, estimated changes in IQR (*middle*) are similar to changes in standard deviation seen in Figures 5 and 6. Changes in tail variability are clearly different from those in IQR, meaning that future distributions are not simply a rescaling of the present-day distributions.

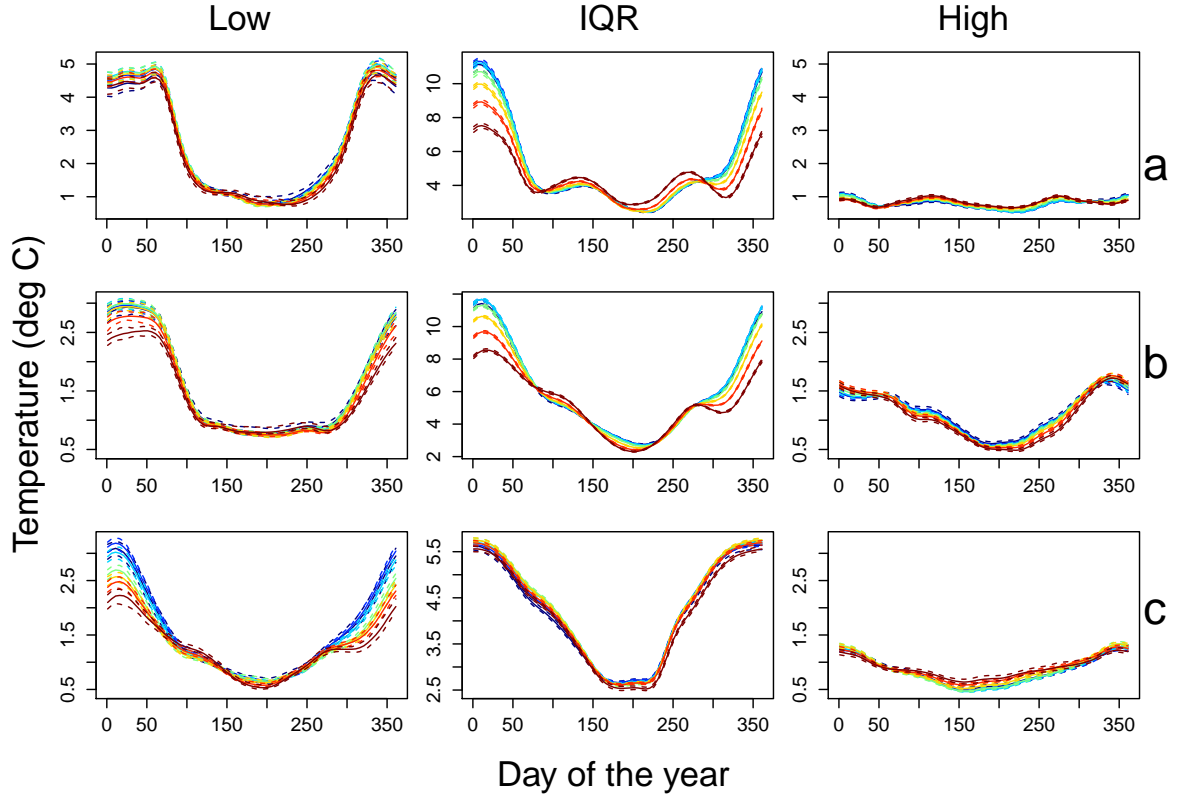


FIG. 8. Evolving daily temperature variability (quantile differences) over time in CESM ensemble RCP8.5 runs estimated using our statistical approach, for locations **a**, **b**, and **c**. Using the analysis described in Figure 7, we show absolute IQR and tail variability as a function of seasonality, with different years (at 40 year intervals) shown as different colored lines, from 1850 (dark blue) to 2090 (dark red). Dashed lines represent pointwise 90% confidence intervals. Note the complexity of seasonal cycles in variability at different locations. These results show that the dipole pattern of changes in wintertime skewness changes seen in Figure 5 is driven by low rather than high tail behavior. In wintertime, in the more northern locations **a** and **b**, IQR reduces more strongly than does low tail variability, making skew more negative. In the more southern location **c**, IQR change is negligible while low tail variability reduces strongly, making skew more positive. In all locations, absolute changes in wintertime low tail variability are larger than changes in high tails. For fractional changes, see Supplementary Online Material Figure S6.

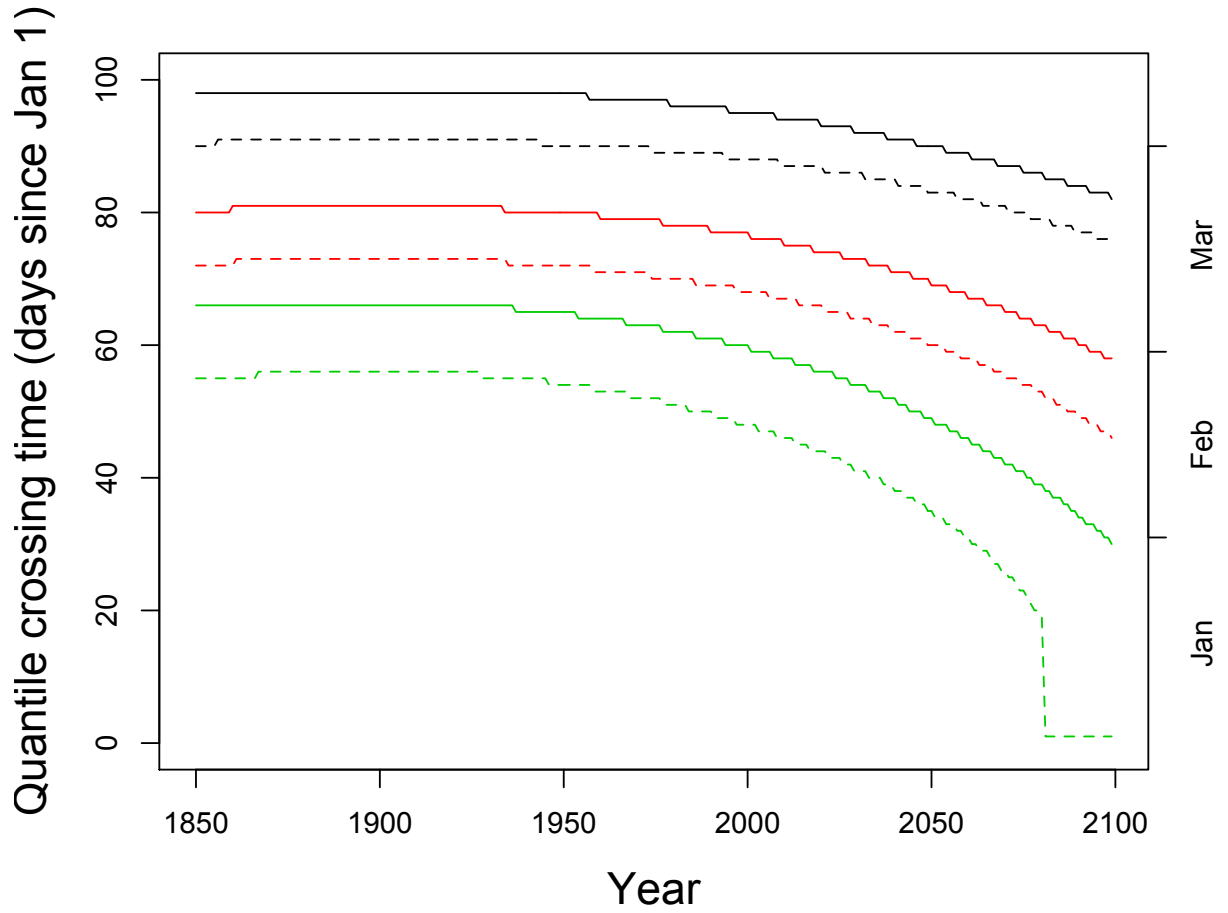


FIG. 9. First day above freezing (solid lines) and -2.2°C (dashed lines) for each year from 1850-2100 as measured by fitting quantiles to average daily temperature of the CESM ensemble data set. Three quantiles are shown to capture the spread of the distribution, 0.5 (green), 0.25 (red) and 0.05 (black).

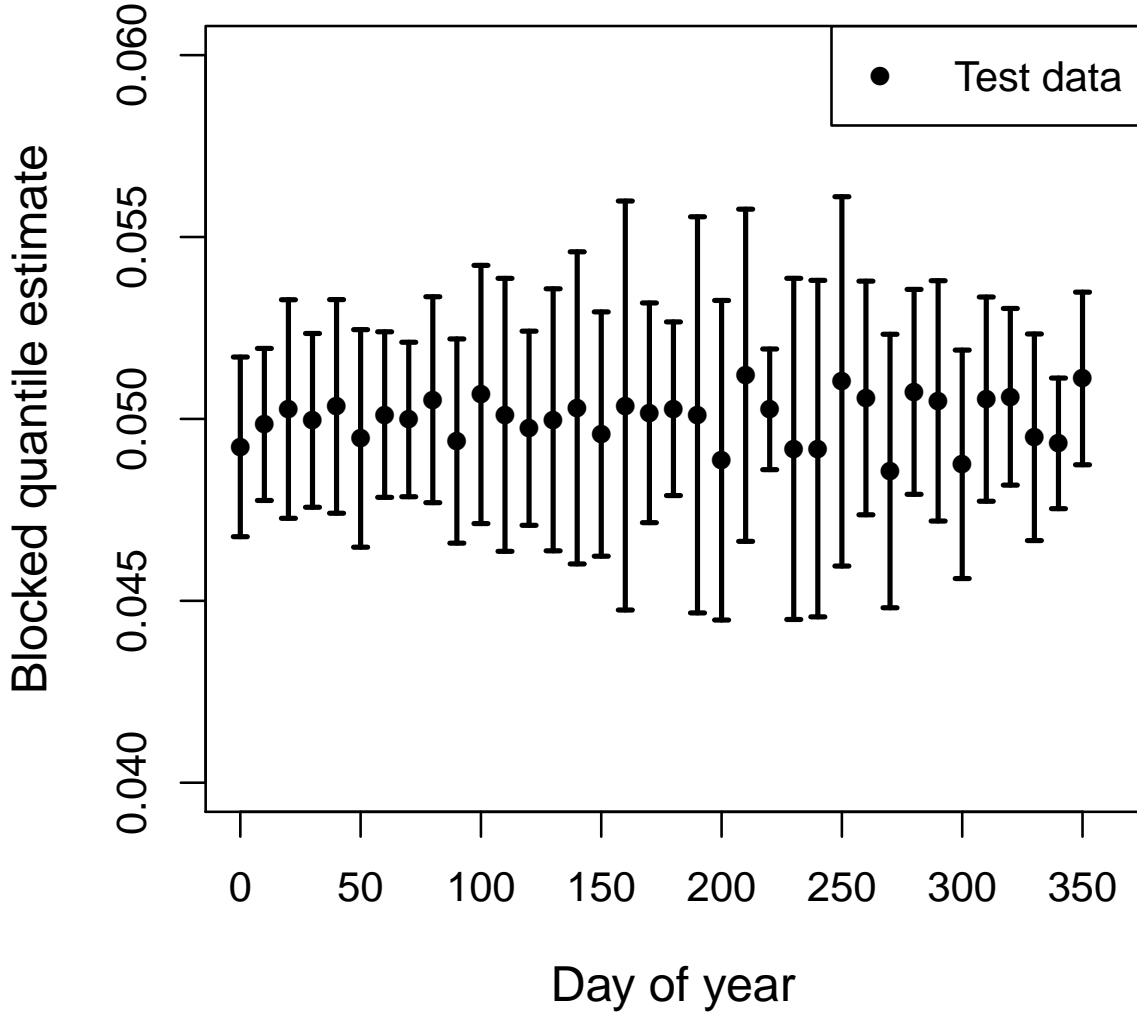


FIG. 10. Exceedence probability of temperature events above the .95 quantile estimate. The density is obtained by making 10-day bins and counting the number of observations that are above the quantile estimate and normalizing by the total number of exceedences aggregated across all model runs. Each bin is represented by the bin start day, i.e. an x-axis value of 0 includes the interval $(0, 10]$. We hold out 10 different sets of simulations to obtain 10 different estimates for each block of time, from which we calculate their mean shown as points and standard deviation shown as error bars around \hat{S}_{test} .

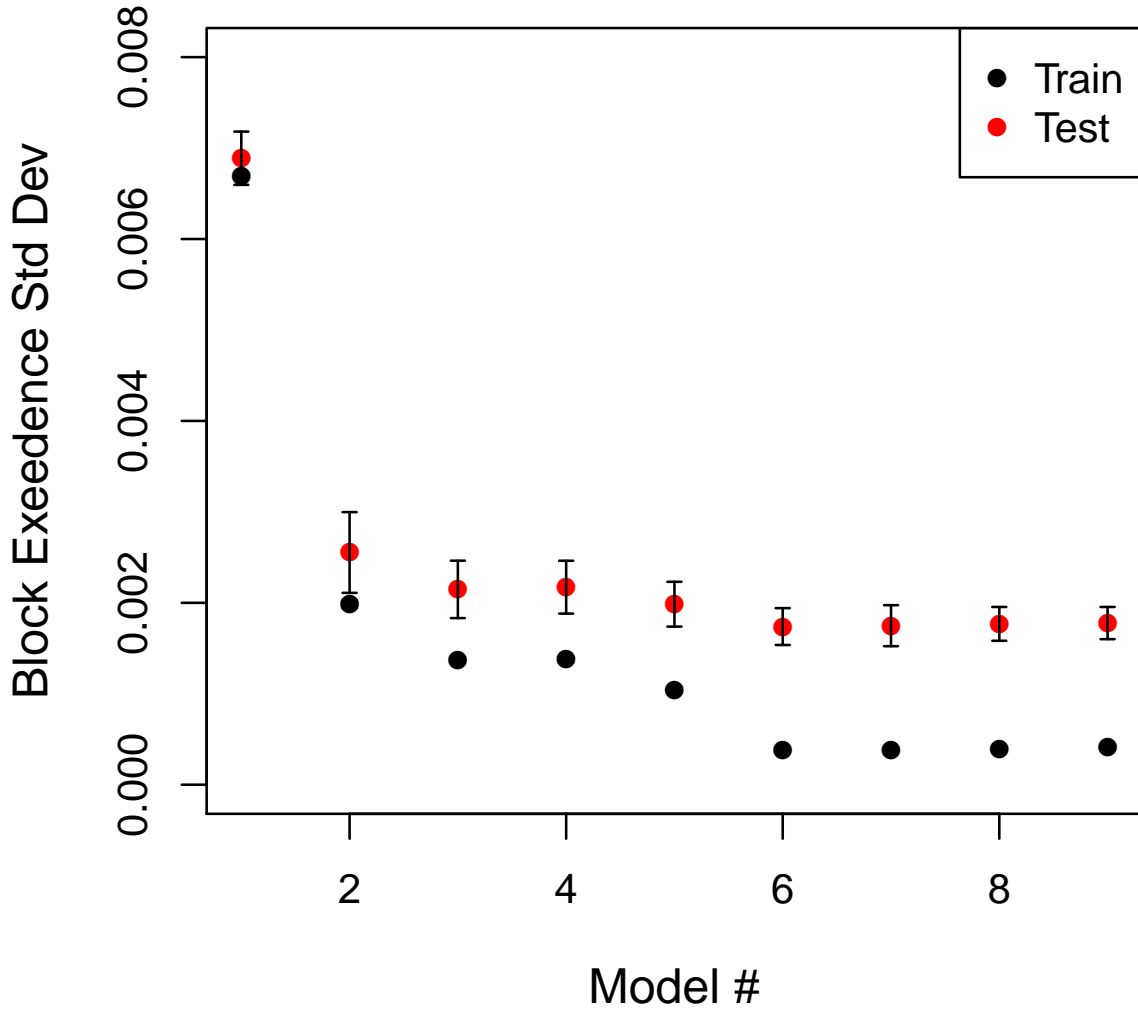


FIG. 11. Training and test exceedence standard deviation as a function of model number, where increasing model number signifies increasing degrees of freedom in the spline basis functions. The data were extracted from the gridbox located at (lat, lon) = (31.5, -93.8). The exceedence is calculated by binning seasonality in 10-day blocks and summing over the long term change.